



Structure analyses and ferroelectric behaviour of barium titanate-doped glass–ceramic nanocrystals for energy storage applications

M. M. El-Desoky¹ · Ibrahim Morad^{1,2,3,4} · H. Elhosiny Ali^{2,3} · F. A. Ibrahim⁴

Received: 28 October 2022 / Accepted: 6 February 2023 / Published online: 16 February 2023
© The Author(s), under exclusive licence to Springer-Verlag GmbH, DE part of Springer Nature 2023

Abstract

New glass–ceramic (GC) nanocrystals of $x\text{BaTiO}_3-(80-x)\text{V}_2\text{O}_5-20\text{PbO}$ glasses (where $x=5, 10, 15, 20$ and 25 mol%) were synthesized via heat treatment at crystallization peak temperature (T_p) according to DSC thermograms. XRD together with dielectric measurements and E-P hysteresis loop were used to evaluate the microstructural and ferroelectric characteristics. Combining these methods made it feasible to improve the conditions for the production of the obtained nanomaterial and to identify correspondences among its nanostructure and ferroelectric features. The ability of appropriate heat treatment to transform glasses into nanocrystalline materials with crystallites smaller than 60 nm embedded in the glassy matrix was demonstrated by XRD measurements. The present glasses' fulfilled dielectric constant values do not show any ferroelectric behavior. Nevertheless, by thermal treatment of the glass system at T_p , GC nanocrystals exhibited an average broad peak of around 330 K in the dielectric constant. The Curie temperature of BaTiO_3 with particle size smaller than 100 nm is extremely close to the average Curie temperature of 338 K measured in the current glass system. By properly adjusting heat-treatment time and BaTiO_3 content, this finding of these samples can be employed to manage BaTiO_3 crystal size and, consequently, transition temperature. As a result, the glass–ceramic samples segregated with nanocrystalline BaTiO_3 are supported by this result's dipolar direction and phase transition. A GC nanocrystal has an intentional energy storage density of 104 mJ cm^{-3} . These findings indicate that the current glass–ceramic nanocrystals are a promising material for creating energy storage devices.

Keywords DSC · XRD · Ferroelectricity · Barium titanate · Glass–ceramic nanocrystals · Glasses · Dielectric constant

1 Introduction

Through the quick improvement of multilayer ceramic capacitors in current years, high dielectric materials with very small grains, in particular, nanosized BaTiO_3 and PbTiO_3 have been used to meet the increasing request for

miniaturization. The synthesis of many ferroelectric materials by nanocrystallization of glass has been discussed in recent years [1–5]. This technique has been useful for various ferroelectric nanocrystals, such as BaTiO_3 , PbTiO_3 , NaNbO_3 , LiTaO_3 , and LiNbO_3 . This technique is simple, economical, and possibly suitable for energy storage devices [6, 7].

In the early stage of crystallization, a structure of nanocrystals was distributed in the glass matrix, so-called glass–ceramic (GC) nanocrystals [8–15]. The benefits of ferroelectric glass–ceramic, such as homogeneous mixing temperature of ferroelectric phases with glass, have been used in ferroelectric applications. Glass ceramic nanocrystals are significant because of their new properties which are not available in other materials. It is essential to study these properties to know their physical properties and to have well device efficiency. Though BaTiO_3 has been a topic of deep investigation, there is still a deficiency in the investigation of

✉ M. M. El-Desoky
mmdesoky@suezuniv.edu.eg; mmdesoky@gmail.com

¹ Department of Physics, Faculty of Science, Suez University, Suez 43518, Egypt

² Department of Physics, Faculty of Science, King Khalid University, P. O. Box 9004, Abha, Saudi Arabia

³ Department of Physics, Faculty of Science, Zagazig University, Zagazig, Egypt

⁴ Department of Physics, Faculty of Science, El-Arish University, Al-Arish, Egypt

the ferroelectric properties of BaTiO₃-related glass–ceramic nanocrystals [16].

Batteries, electrochemical supercapacitors, and dielectric capacitors are some of the current clean and renewable energy sources. Batteries and fuel cells often have high energy storage densities comparable to dielectric capacitors however low high-power output. Supercapacitors can achieve great energy and power densities, however, the lengthy charge–discharge process might occasionally impair their performance. Nevertheless, the upsides of high power density, faster charge–discharge rates, and high efficiency of dielectric capacitors expand their use in electronic devices, pulsed power supplies, and power systems, such as electromagnetic guns, inverter equipment, hybrid electric vehicles, military launch platforms, etc. [17, 18]. The limited energy density, tiny discharge currents, and limited lifetime of currently utilised commercial capacitors made of dielectric polymers and ceramics restricts their utilisation. These materials fall short of meeting the requirements for a high energy storage density, which include having a high dielectric break-down strength (BDS) and low dielectric losses. For instance, ferroelectric ceramics have low BDS but high dielectric constants. Similar to BDSs, dielectric polymers have low dielectric constants but high BDSs, which restricts their use in the relevant sectors [19]. Currently, the necessity for electronic and electrical equipment upgrading necessitates the development of small, light, affordable, and high-energy storage capacities. Therefore, the development of dielectric materials with a high energy storage density depends on material composition, dielectric behaviour (linear, ferroelectric, and antiferroelectric), synthesis, and fabrication procedures [20].

Glass–ceramics hold great potential for this industry. They grow as a result of carefully regulated glass crystallisation. Crystals are dispersed throughout their structures in a transparent matrix [21]. These substances combine the characteristics of glass (easiness of elaboration and formatting, lack of porosity, transparency) with the unique characteristics of the crystalline phase (strong electric breakdown field, increased permittivity, etc.). For illustration, silicate SrO–TiO₂–Al₂O₃–SiO₂ glass–ceramics are known to have energy storing capabilities [22].

In our recent work [3], the microstructural and ferroelectric characteristics of BaTiO₃–V₂O₅ glasses and glass ceramic nanocrystals were studied. TEM of glass ceramic nanocrystals of these samples showed nanocrystals with a crystal size of 20–35 nm. It was found that from the dielectric permittivity of the as-cast glass samples no ferroelectric behavior can be observed. By annealing these glasses around crystallization temperature for 1 h in the air, nanocrystalline BaTiO₃ phase precipitates and the corresponding nanocrystalline glass–ceramics showed an average broad peak around 352 K in the dielectric permittivity (ϵ). This observation of

these glass–ceramics nanocrystals can be utilized to control BaTiO₃ particle size and hence transition temperature by proper adjustment of annealing time and BaTiO₃ content. Such a feature can be used for industrial applications where the shape of the application article is an essential requirement.

However, the high energy storage density in 60Bi₂O₃–10SrO–30Fe₂O₃ glass is for designing high-performance capacitors. Systematically evaluated dielectric properties revealed relaxor ferroelectric-like behavior in a wide range of frequencies and temperatures. The glass sample shows a broad and diffuse peak of dielectric permittivity $\epsilon'(\omega)$. Broad and diffuse peaks shifted to higher temperatures, denoting the typical relaxor behavior. The measured energy storage density of the strontium-doped glass was 4 mJ cm⁻³ with an efficiency of 70% under an applied electric field of 17 kV cm⁻¹ at room temperature (RT) [23].

The main objective of the present work is to investigate two subjects x BaTiO₃–(80– x)V₂O₅–20PbO (where $x=5, 10, 15, 20$ and 25 mol%) glasses. The first is to prepare these glasses and the corresponding glass–ceramics nanocrystals. The second is to investigate the compositional dependence of the nanostructure and temperature-dependent dielectric and ferroelectric properties of the glasses and glass–ceramic nanocrystals, obtained by partial heat treatment at crystallization temperature for 1 h.

2 Experimental technique

2.1 Sample preparation

BaTiO₃ (Alfa Aesar, 99.99%), V₂O₅ (Alfa Aesar, 99.999%), and PbO (Alfa Aesar, 99.8%) of reagent grade raw materials were weighed in the adequate amounts, 12 g intimate level melded with ethanol in an agate mortar to guarantee homogeneous raw materials distribution, and then heated at 700 °C for 6 h in a platinum crucible specifically to remove any extra organic materials. The combination was then melted for 60 min at 1100 °C in an electrical muffle furnace. The melt was then promptly quenched by pressing with another copper block of a comparable size after being poured onto a thick copper block. After this process, we were able to generate bulk glass that was 1 mm thick and 2 × 2 cm in size. The aforesaid glasses were heated in the air at the crystallization temperature of T_p for one hour in order to crystallize the glass–ceramic nanocrystal composite.

2.2 Sample characterizations

Shimadzu differential scanning calorimeter (DSC) 50 instrument DSC analyses were used to determine the glassy specimens' crystalline regime. The structure for the glass

(G) and glass ceramic (GC) was examined by X-ray diffraction (XRD) patterns using X-ray diffractometry (Shimadzu XRD-6000) instrument with Cu K α radiation ($\lambda = 1.5418 \text{ \AA}$). The diffraction data were documented for 2θ between 10° and 80° with a resolution of 0.02.

2.3 Set up of ferroelectric experiments

Electrodes made of silver paste were applied to the polished samples on both faces. On the contrary, ferroelectric parameters including dielectric permittivity were measured using an LCR meter spanning the frequency range of 0.12–1 kHz up to 473 K from room temp. The ferroelectric hysteresis loops (P–E) of the sample were evaluated at 50 Hz with a Sawyer–Tower circuit.

3 Results and discussion

3.1 Structural analysis

3.1.1 DSC

Figure 1 displays the differential scanning calorimeter (DSC) thermogram for $20\text{BaTiO}_3\text{--}60\text{V}_2\text{O}_5\text{--}20\text{PbO}$ glass. Depending on the DSC curve, glass transition temperature (T_g), crystallization temperature (T_p), and melting temperature (T_m). The temperature difference $\Delta T = T_p - T_g$ for the present glass system which displays the thermal stability was calculated. The crystallization is indicated by the exothermic peak in the $325\text{--}363^\circ\text{C}$ temperature range and the peak locations are designated as the crystallization peak temperature of T_p . At $254\text{--}276^\circ\text{C}$, the endothermic dip associated with the glass transition (T_g) is seen. Additionally, at $490\text{--}535^\circ\text{C}$, melting temperature (T_m)-induced endothermic dips are observed.

The glass transition temperature T_g rises with increasing BaTiO_3 content, indicating that the non-bridging oxygen's (NBO) contribution to the current glass system is reduced. It is revealed that the crystallization temperature (T_p) rises approximately linearly as the percentage of BaTiO_3 increases [3]. On the contrary, DSC research [24] on the microstructure of several glasses has indeed demonstrated that T_g exhibits a clear association with the modification of the network former's coordination number and the creation of NBO atoms, which indicates the network structure breakdown [25]. T_g often exhibits a clear increase as the network former's coordination number rises. In contrast, an NBO construction results in a T_g reduction. As a result, the steady rise in T_g in the current system indicates that the number of V^{5+} and V^{4+} ions that can coordinate is going to drop and that NBO atoms are being eliminated [26]. Additionally, the rise in T_g shows that the chemical connection between oxygen atoms and metal atoms grows stronger. This is explained by the greater density brought on by the greater interatomic distances among metal and oxygen ions [27].

Figure 1a, b includes the thermal stability factor, ΔT , and its motional dependence. The ΔT value is estimated to be around 79°C , and it grows as the amount of BaTiO_3 in the glasses increases, demonstrating that the glasses' thermal stability increases with BaTiO_3 concentration. The T_g/T_m ratio can also be used to determine the stability of glasses. The optimum T_g/T_m value for exceptionally robust glass is 0.67 [28]. All the compositions tested in the current system had T_g/T_m values between 0.51 and 0.52, which are close to the ideal value.

3.1.2 XRD

A typical X-ray diffraction pattern (XRD) of the glass $20\text{BaTiO}_3\text{--}60\text{V}_2\text{O}_5\text{--}20\text{PbO}$ and the associated glass–ceramic

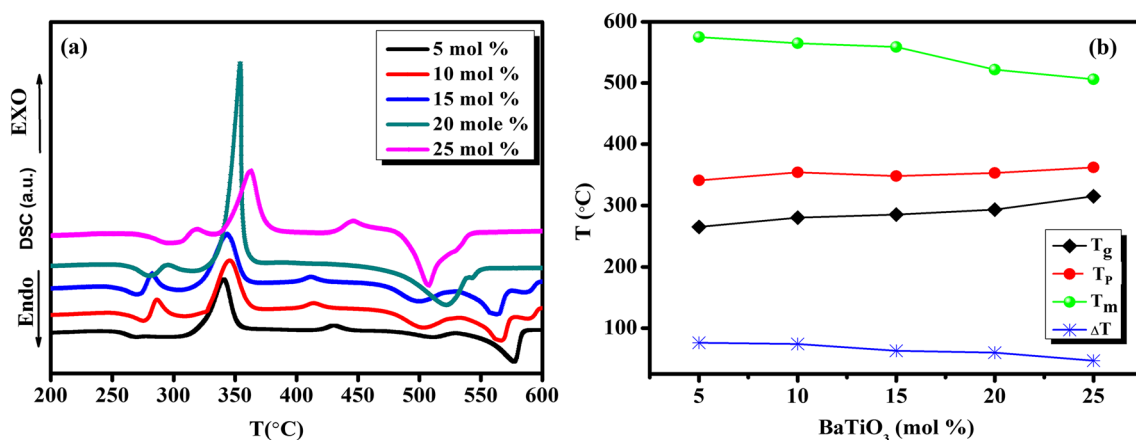


Fig. 1 a DSC thermogram for $x\text{BaTiO}_3\text{--}(80\text{--}x)\text{V}_2\text{O}_5\text{--}20\text{PbO}$ glasses (where $x = 5, 10, 15, 20$ and 25 mol\%), b The DSC dependence of composition T_g , T_p , and T_m temperature difference (ΔT) for various glass compositions

nanocrystals are shown in Fig. 2a,b. As presented in Fig. 2, the absence of any diffraction peaks and the domination of broad hump suggest the dominance of the glassy phase on the as-prepared glass sample. This supports the original glasses' amorphous state theory. There are still significant amounts of amorphous phase in the samples that had a one-hour heat treatment at T_p because they contain several peaks representing nanocrystalline phases superimposed on a wide periphery. The heat-treated sample's XRD pattern shows unequivocally that annealing at temperature T_p only begins to result in tiny nanocrystallites which are attributed to $Ba_3TiV_4O_{15}$ (JCPDS-00-036-1488), $BaTiO_3$ (PDF#83-1875), V_2O_5 (PDF#86-2248), and PbO (PDF#85-1287) in the glass matrix [12, 29, 30]. In addition, some additional peaks are associated with the phase that we have not yet detected. This is a significant insight since it implies that one can manage the volume of nanocrystalline grains that form in the material and so improve its electrical conductivity by controlling the annealing temperature. Using the Scherrer formula [31, 32], the average size of nanocrystallites may be predicted from the widths of diffraction peaks to a maximum of 50 nm. According to X-ray line-broadening measurements, the crystal size of $BaTiO_3$ and V_2O_5 have an average size of 40–60 nm. Similar results were obtained in the other samples.

3.2 Ferroelectric properties

3.2.1 Dielectric properties

The real part of the dielectric constant (ϵ) for the current glasses is shown in Fig. 3 as a function of temperature from room temperature up to 473 K at selected frequencies. The real part of the dielectric constant (ϵ) is calculated from the formula $\epsilon(\omega) = C_p/C_o$ (C_p is the measured parallel

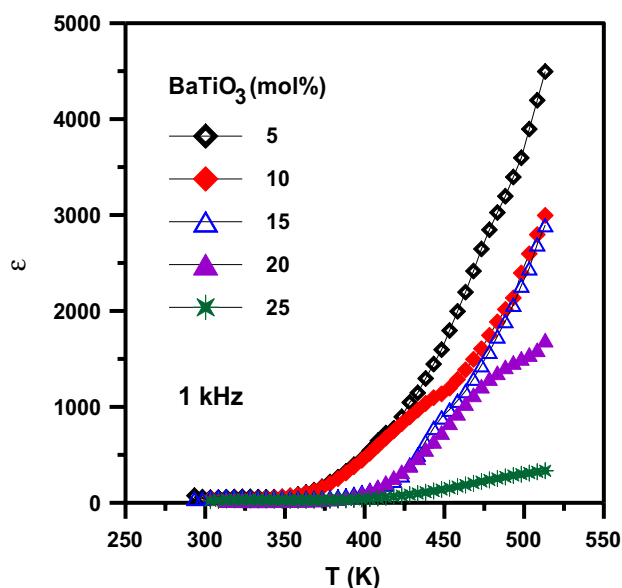


Fig. 3 Temperature reliance of dielectric constant for $xBaTiO_3-(80-x)V_2O_5-20PbO$ glasses (where $x=5, 10, 15, 20$ and 25 mol%)

capacitance and C_o is the vacuum capacitance). Figure 3 depicts the dielectric constant's temperature dependency for the glass matrix at a specific frequency (1 kHz). This figure demonstrates that the glass samples in their as-cast state do not exhibit any ferroelectric response. The fact that these glasses exhibit high dielectric constants in comparison to pristine V_2O_5 , pure Bi_2O_3 , and pure crystalline $BaTiO_3$ is also interesting to notice [15]. These glasses' high dielectric constants are thought to be a result of the tiny nanocrystals $Ba_3TiV_4O_{15}$, $BaTiO_3$, and V_2O_5 that are embedded in the glass matrix [3]. According to Sadhukhan et al. [33], nanocrystalline TiO_2 has a dielectric constant that is multiple orders of magnitude higher than bulk TiO_2 . Therefore,

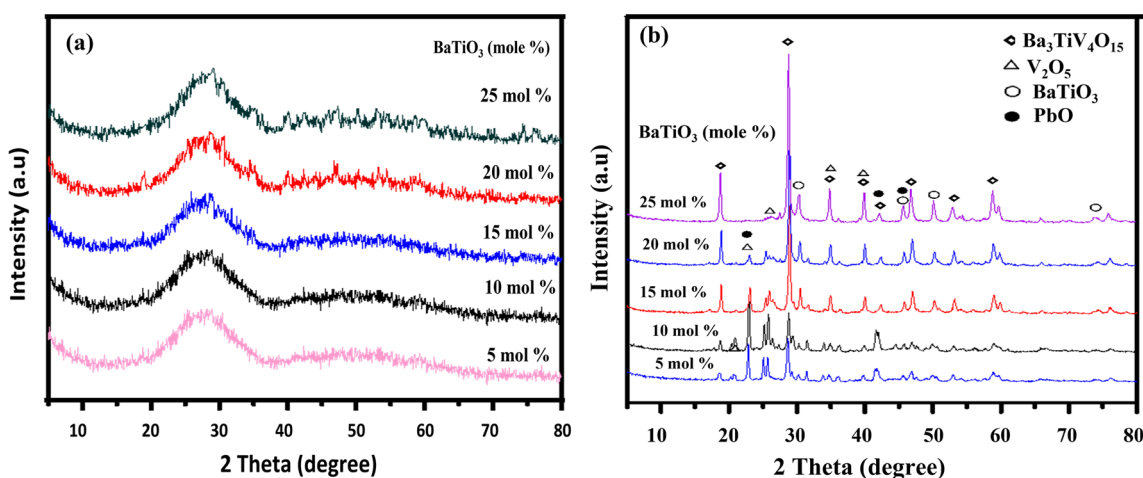


Fig. 2 XRD for a $xBaTiO_3-(80-x)V_2O_5-20PbO$ glasses (where $x=5, 10, 15, 20$ and 25 mol%) and b corresponding GC nanocrystals

the inclusion of nanocrystalline Ba₃TiV₄O₁₅, BaTiO₃, V₂O₅, and Bi₂O₃ grains or clusters inside the glass matrix could be responsible for the high dielectric constant values of the present glasses. The decrease in bond energies is typically correlated with the increase in the dielectric constant of the samples with temperature [40]. That is, when the temperature rises, there may be two impacts on the dipolar polarization: (i) deterioration of the intermolecular interactions that improve the orientational vibration, and (ii) a severe disturbance of the orientational vibrations because of a rise in thermal agitation.

Now that we have confined our focus to one frequency of 1 kHz, we can compare the data from all the glass–ceramic nanocrystals. In the 293–513 K temperature range, the dielectric constant was evaluated for various compositions. For various GC nanocrystal compositions, the fluctuation of temperature at 1 kHz is illustrated in Fig. 4. Ferroelectric to paraelectric phase transitions were visible in all of the compositions. Figure 5 illustrates how the dielectric constant for a particular batch of 15BaTiO₃–65V₂O₅–20PbO GC nanocrystals varies with temperature at various frequencies. For all frequencies, it is noted that the sample of glass–ceramic nanocrystals has a higher dielectric constant than that of the glass as received (0.12–100 kHz). The glass–ceramic nanocrystal samples’ greater dielectric constant value is suggestive of the presence of potent dipolar interactions in the glass matrix. In order to grasp the nature of the anomalies/transition, we were tempted to adopt the analysis that is typically used. In contrast, the dielectric constant rises with temperature and shows a distinct broad peak

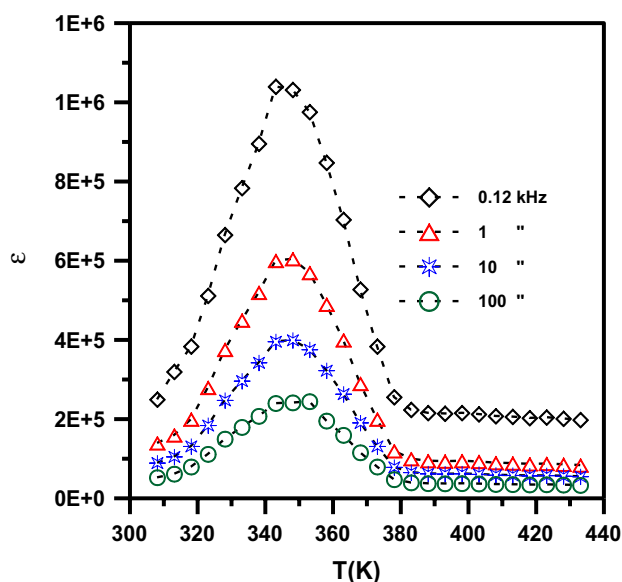


Fig. 5 Dielectric constant as a function of Temperature at different frequencies for 15BaTiO₃–65V₂O₅–20PbO GC nanocrystals

at roughly 338 K for all the frequencies being investigated. In contrast, the dielectric constant rises with temperature and shows a distinct broad peak at roughly 338 K for all the frequencies being investigated. By increasing the measurement frequency, no discernible change in the peak position was found. The phase transition (Curie) temperature of GC nanocrystals composed of barium titanate is thought to be responsible for the anomaly that was discovered at this temperature [3].

Furthermore, the glass–ceramic nanocrystals system is extremely comparable to the materials that could be associated with the dielectric behavior in terms of interpretations that are typically employed in dealing with polar materials that show dispersed phase transitions (DPT). The fundamental distinction is that the transition observed here is connected to the nanocrystallites that are diffused throughout the glass matrix. It is well-recognized that nanostructures have a significant impact on the dielectric, polar, and phase transition characteristics of GC [34]. By supposing that the ferroelectric in the paraelectric phase complies with Curie–Weiss’s Law given by Eq. 1 [35, 36], one can theoretically assess how the dielectric constant varies with temperature.

$$\epsilon = \frac{C}{T - T_o} \tag{1}$$

where *C*, *T_o*, and *T* are the Curie constant, Curie–Weiss temperature in *K*., and absolute temperature, respectively. The plot of 1/ε against *T* is recognized to provide for the prediction of the type of phase transition that arises in

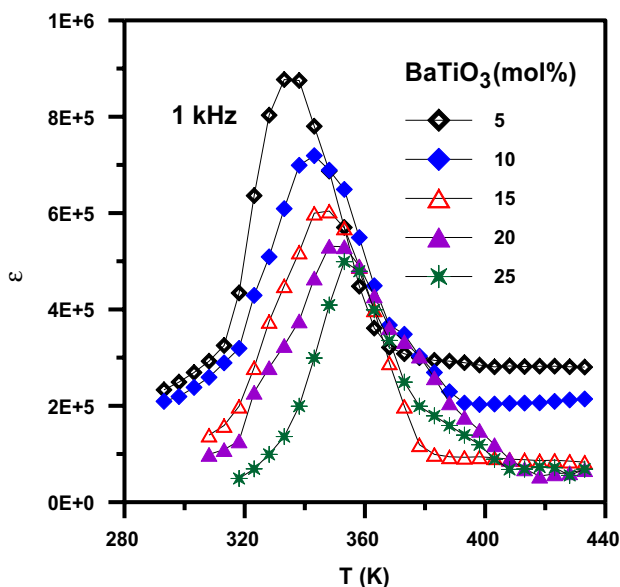


Fig. 4 Dielectric constant as a function of Temperature at (1 kHz) frequency for *x*BaTiO₃–(80–*x*)V₂O₅–20PbO (where *x*=5, 10, 15, 20 and 25 mol%) GC nanocrystals

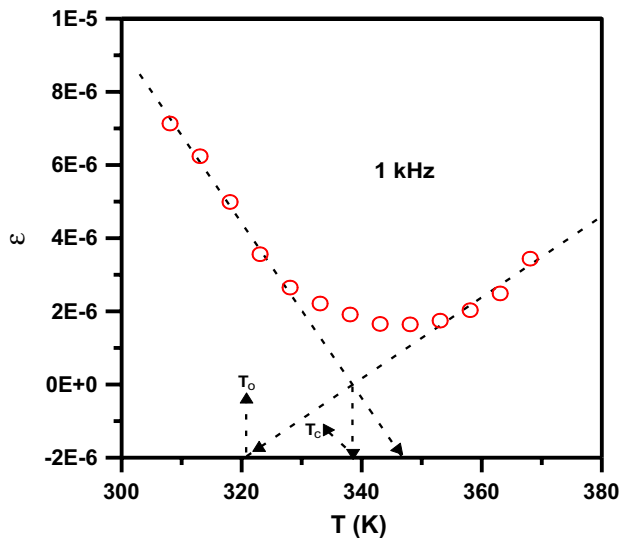


Fig. 6 Curie–Weiss law for 15BaTiO₃–65V₂O₅–20PbO GC nanocrystals

ferroelectric materials. Plots of $1/\epsilon$ versus T for representative 15BaTiO₃–65V₂O₅–20Bi₂O₃ glass–ceramic nanocrystals are shown in Fig. 6. The graph makes it evident that a linear zone over 338 K is shown at 1 kHz, indicating that the dielectric constant accepts the Curie–Weiss equation at all temperatures over the transition point. The curve in Fig. 6 can be separated into three parts if we compare this type of behaviour to that of a ferroelectric with a diffuse phase transition. According to the Curie–Weiss relation, the first zone depicts a ferroelectric behavior up to the transition T_c , the second region closer to the transition denotes a diffuse transition, and the third region depicts a linear behavior of $1/\epsilon$ Vs T in the paraelectric phase. Regarding a particular example of the composition 15BaTiO₃–65V₂O₅–20PbO with Curie–Weiss constant $C = 1.8 \times 10^6$ K, Curie temperature $T_c = 338$ K and Curie–Weiss temperature $T_o = 320$ K as shown in Fig. 7. As an instance, the parameter $n = -2.2$, in which n is the ratio of the two slopes of the curves in Fig. 7 below and above T_c , respectively, indicates almost a second order phase transition. Whereas this Curie constant, $C = 1.8 \times 10^6$ K, is a sign of fine dispersion ferroelectric material [37], and the identical order of magnitude of BaTiO₃–V₂O₅ GC nanocrystals. These parameter values are essential for utilizing the substance in any device, nevertheless. On the other hand, Fig. 7 illustrates how the critical Curie temperature, T_c , varies as a function of the amount of BaTiO₃, suggesting that T_c shifts upward as BaTiO₃ content rises. The current system’s average Curie temperature of 338 K is quite similar to the Curie temperature of pure BaTiO₃ with grains smaller than 100 nm [38, 39]. Due to the stress placed on the particle–glass interfaces, isolated barium titanate particles with grain sizes of 40–60 nm that crystallized out of a glass

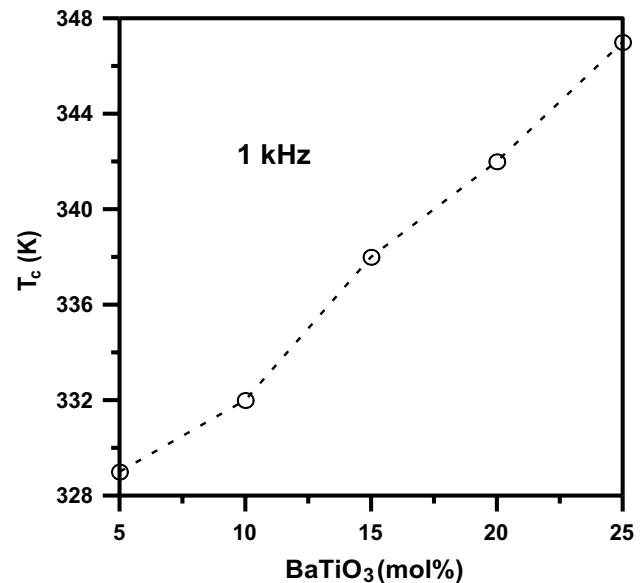


Fig. 7 The Curie temperature as a function of BaTiO₃ content in the x BaTiO₃–(80– x)V₂O₅–20PbO (where $x = 5, 10, 15, 20$ and 25 mol%) GC nanocrystals

matrix exhibit a ferroelectric response that can be asserted to have transpired.

As a result, the size of the BaTiO₃ nanocrystals and the boundary conditions in which they occur to influence the critical behavior of barium titanate (ferroelectric—paraelectric transition and shift from monodomain to polydomain structure). The process of preparing the powder or polycrystalline material determines the size of the particle or grain and the boundary conditions (mechanical stress, depolarizing field, etc.). It’s fascinating to observe that the pure nanocrystalline BaTiO₃ phase, with average particle sizes just under 100 nm, undergoes a ferroelectric phase transition at this temperature, in accordance with predictions made from determinations of the dielectric permittivity. Nevertheless, the diffuseness of the dielectric property of the current samples closes the phase transition temperature may be believed to be due to the irregular distribution of charged defects or impurities (in this case, impurity phases like BaTiO₃), which could result in large-scale potential or polarization variability. As a result, it is reasonable to suppose that the glass–ceramic nanocrystal materials under study are an amalgamation of nano/micro-regions with various instances. Accordingly, rather than occurring at a specific temperature, the phase transition proceeds throughout a range of temperatures, which accounts for the noted DPT behavior [34]. Finally, by carefully adjusting the annealing period and BaTiO₃ content, this observation of these glass–ceramic nanocrystals can be utilized to regulate BaTiO₃ particle size and, consequently, transition temperature. For the employment

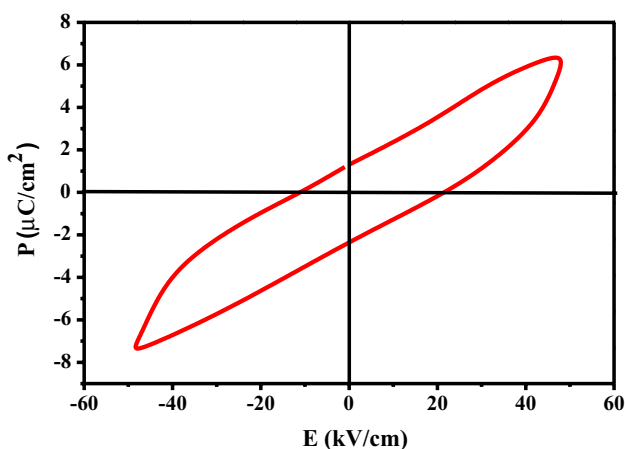


Fig. 8 P–E hysteresis loop at RT for 15BaTiO₃–65V₂O₅–20PbO GC nanocrystals

of the substance in either technology, the values of these factors are crucial.

3.2.2 P–E hysteresis loop

The effectiveness of the produced glass sample’s ability to store energy is investigated using the polarization–electric field (P–E) hysteresis loop. P–E loops of a delegate representative sample of 15BaTiO₃–65V₂O₅–20PbO GC nanocrystals, collected at a frequency of 50 Hz, are presented in Fig. 8. The glass displays a typical ferroelectric-like shaped loop with a significant P_r and E_c at ambient temperature. The loop displays a remnant polarisation P_r of around 0.126 $\mu\text{C cm}^{-2}$, maximum polarisation P_{max} of about 6.4 $\mu\text{C cm}^{-2}$, and a coercive field E_c of approximately 21.46 kV cm^{-1} . P–E loop measurements are used to estimate the energy storage density W_r , as shown below [40, 41]:

$$W_r = \int_{P_r}^{P_{\text{max}}} E dP \tag{2}$$

where P_{max} and P_r represent the polarization at the maximum applied field E_{max} and remnant polarization, respectively, E stands for the applied electric field and P corresponds to the polarization. The GC sample composed of 15BaTiO₃–65V₂O₅–20PbO exhibits an energy density of around 104.9 mJ cm^{-3} .

The following formula Eq. 3 [42] can be used to evaluate the glass sample’s efficiency (η)

$$\eta = \left(\frac{W_r W_r}{+ WL} \right) \eta = \left(\frac{W_r}{W_r + W_L} \right) \times 100 \tag{3}$$

where w_L symbolizes the energy loss (hysteresis loop area). The glass sample’s efficiency (η) is around 73% at room

temperature. Dielectric materials having a big polarization difference $\Delta P = P_{\text{max}} - P_r$, large W_r , and high efficiency are typically indispensable for high-performance capacitors. These findings demonstrate that glass–ceramic nanocrystals are a promising candidate for creating energy storage devices presently [40, 41].

4 Conclusion

By annealing at T_p for one hour, the glass system of $x\text{BaTiO}_3 - (80-x)\text{V}_2\text{O}_5 - 20\text{PbO}$ glasses (where $x = 5, 10, 15, 20$ and 25 mol%) has been transformed into glass–ceramic (GC) nanocrystals. The current system’s dielectric constant value does not exhibit any ferroelectric behaviour. On the other hand, by annealing the current glass system at T_p for 1 h, the ϵ increases with the temperature rise exhibit a definite broad peak at roughly 338 K. No obvious change in the peak location has been revealed by increasing the measurement frequency. The anomaly showed at T_c is supposed to be accompanying the phase transition (Curie) temperature of BaTiO₃ doped GC nanocrystals. The Curie temperature T_c was enhanced by raising the BaTiO₃ content. The average parameter $n = -2.2$ value displayed a practically second-order phase transition. The average value of the Curie constant, $C = 1.8 \times 10^6$ K, is evidence of displacive ferroelectric nanomaterial. At ambient temperature, the polarization–electric field (P–E) hysteresis loop for the glass sample under study shows a ferroelectric-like shape loop, owning a 104.9 mJ cm^{-3} energy density. Nonetheless, for the material to be used in any energy storage device, the values of these characteristics are crucial.

Acknowledgements The authors extend their appreciation to the Ministry of Education in KSA for funding this research work through the project number KKU-IFP2-DA-5.

Availability of data and materials All data generated or analyzed during this study are included in this article. Requests for material should be made to the corresponding author (M. M. El-Desoky).

Declarations

Conflict of interest The authors declare that there is no conflict of interest in the current article.

References

1. H.C. Zeng, K. Tanaka, K. Hirao, N. Soga, J. Non-Cryst. Solids. **209**, 112–121 (1997)
2. M.V. Shankar, K.B.R. Varma, J. Non-Cryst. Solids. **226**, 145–154 (1998)
3. M.S. Al-Assiri, M.M. El-Desoky, A. Al-Hajry, A. Al-Shahrani, A.M. Al-Mogeeth, A.A. Bahgat, Phys. B. **404**, 1437–1445 (2009)
4. A.E. Harby, A.E. Hannora, M.S. Al-Assiri, M.M. El-Desoky, J. Mater. Sci. **27**, 8446–8454 (2016)

5. L. Lin, J. Huang, W. Yu, L. Zhu, H. Tao, P. Wang, Y. Xu, Z. Zhang, J. Magn. Magn. Mater. **500**, 166380 (2020)
6. N. Syam Prasad, K.B.R. Varma, J. Non-Cryst. Solids. **351**, 1455–1465 (2005)
7. Y. Hu, C.L. Huang, J. Non-Cryst. Solids. **278**, 170–177 (2000)
8. Montagne, L., L. Cormier, and D. Caurant, 25. *Bibliographie*, in *Du verre au cristal*. EDP Sciences, 501–578 (2021)
9. B.C. Babu, B.V. Rao, M. Ravi, S. Babu, J. Mol. Struct. **1127**, 6–14 (2017)
10. M.M. El-Desoky, F.A. Ibrahim, A.G. Mostafa, M.Y. Hassaan, Mater. Res. Bull. **45**, 1122–1126 (2010)
11. M.M. El-Desoky, Mater. Chem. Phys. **119**, 389–394 (2010)
12. J. Garbarczyk, P. Jozwiak, M. Wasiucioneck, J. Nowinski, J. Power Sour. **173**, 743–747 (2007)
13. N. SyamPrasad, K.R. Varma, Y. Takahashi, Y. Benino, T. Fujiwara, T. Komatsu, J. Solid State Chem. **173**, 209–215 (2003)
14. M.M. El-Desoky, Phys. Stat. Sol. (A). **195**, 422–428 (2003)
15. K. Tanaka, K. Kashima, K. Hirao, N. Soga, A. Mito, H. Nasu, J. Non-Cryst. Solids. **185**, 123–126 (1995)
16. Y. Ohta, M. Kitayama, K. Kaneko, S. Toh, F. Shimizu, K. Morinaga, J. Am. Ceramic Soc. **88**, 1634–1636 (2005)
17. L.A. Thomas, Ferroelectrics **3**, 231–238 (1972)
18. A.S. Aricò, P. Bruce, B. Scrosati, J.-M. Tarascon, W. van Schalkwijk, Nat. Mater. **4**, 366–377 (2005)
19. X. Hao, J. Adv. Dielect. **03**, 1330001–1330009 (2013)
20. L. Yang, X. Kong, F. Li, H. Hao, Z. Cheng, H. Liu, J.-F. Li, S. Zhang, Progress Mater. Sci. **102**, 72–108 (2019)
21. J.E. Shelby, *Introduction to glass science and technology* (Royal Society of Chemistry, 2020)
22. E.P. Gorzkowski, M.J. Pan, B. Bender, C.C.M. Wu, J. Electroceramics. **18**, 269–276 (2007)
23. A.M. Ali, A.E. Hannora, E. El-Falaky, M.M. El-Desoky, J. Non-Cryst. Solids. **584**, 121382 (2022)
24. M. Al-Assiri, S. Salem, M. El-Desoky, J. Phys. Chem. Solids. **67**, 1873–1881 (2006)
25. M. El-Desoky, M. Al-Assiri, A. Bahgat, J. Alloys Compd. **590**, 572–578 (2014)
26. M.M. El-Desoky, M.S. Al-Assiri, Mater. Sci. Eng. B. **137**, 237–246 (2007)
27. N.K. Wally, E. Sheha, B.M. Kamal, A.E. Hannora, M.M. El-Desoky, J. Alloys Compd. **895**, 162644 (2022)
28. S. Sakka, J. Mackenzie, J. Non-Cryst. Solids **6**, 145–162 (1971)
29. M. El-Desoky, F. Ibrahim, A. Mostafa, M. Hassaan, J Mater Res Bull. **45**, 1122–1126 (2010)
30. J.E. Garbarczyk, P. Jozwiak, M. Wasiucioneck, J.L. Nowinski, Solid State Ionics **177**, 2585–2588 (2006)
31. I. Morad, H.E. Ali, M. Wasfy, A. Mansour, M. El-Desoky, Vacuum **181**, 109735 (2020)
32. M. Salah, I. Morad, H.E. Ali, M.M. Mostafa, M.M. El-Desoky, J. Inorg. Organomet. Polym. Mater. **31**, 3700–3710 (2021)
33. M. Sadhukhan, D. Modak, B. Chaudhuri, J. Appl. Phys. **85**, 3477–3487 (1999)
34. W. Xiaoyong, F. Yujun, Y. Xi, Appl. Phys. Lett. **83**, 2031–2033 (2003)
35. Y.M. Poplavko, V. Bovtun, N.N. Krainik, G.Ae. Smolenskii, J. Fizika Tverdого Tela. **27**, 3161–3163 (1985)
36. A.A. Bokov, M. Maglione, A. Simon, Z.G. Ye, Ferroelectrics **337**, 169–178 (2006)
37. M.E. Lines, A.M. Glass, *Principles and applications of ferroelectrics and related materials* (Oxford University Press, 2001)
38. T. Hoshina, H. Kakemoto, T. Tsurumi, S. Wada, M. Yashima, J. Appl. Phys. **99**, 054311 (2006)
39. M. Al-Assiri, M. El-Desoky, J. Non-cryst. Solids. **358**, 1605–1610 (2012)
40. K.A. Shore, Contemp. Phys. **55**, 337–337 (2014)
41. D.J. Thouless, Science **207**, 1196–1197 (1980)
42. J. Wang, N. Sun, Y. Li, Q. Zhang, X. Hao, X. Chou, Ceram. Int. **43**, 7804–7809 (2017)

Publisher's Note Springer Nature remains neutral with regard to jurisdictional claims in published maps and institutional affiliations.

Springer Nature or its licensor (e.g. a society or other partner) holds exclusive rights to this article under a publishing agreement with the author(s) or other rightsholder(s); author self-archiving of the accepted manuscript version of this article is solely governed by the terms of such publishing agreement and applicable law.